New Phytologist

Research

Exploring 3D leaf anatomical traits for C_4 photosynthesis: chloroplast and plasmodesmata pit field size in maize and sugarcane

Moon-Sub Lee[1], Ryan A. Boyd[1], Kingsley A. Boateng[1] and Donald R. Ort[1,2,3]

[1]Carl R. Woese Institute for Genomic Biology, University of Illinois at Urbana-Champaign, Urbana, IL 61801, USA; [2]Department of Plant Biology, University of Illinois at Urbana-Champaign, Urbana, IL 61801, USA; [3]Department of Crop Science, University of Illinois at Urbana-Champaign, Urbana, IL 61801, USA

Author for correspondence:
Donald R. Ort
Email: d-ort@illinois.edu

Received: *1 November 2022*
Accepted: *8 April 2023*

New Phytologist (2023)
doi: 10.1111/nph.18956

Key words: 3D leaf imaging, C_4 photosynthesis, chloroplast, laser scanning microscopy (LSM), plasmodesmata, serial block face scanning electron microscopy (SBF-SEM).

Summary

- Volume and surface area of chloroplasts and surface area of plasmodesmata pit fields are presented for two C_4 species, maize and sugarcane, with respect to cell surface area and cell volume.
- Serial block face scanning electron microscopy (SBF-SEM) and confocal laser scanning microscopy with the Airyscan system (LSM) were used. Chloroplast size estimates were much faster and easier using LSM than with SBF-SEM; however, the results were more variable than SBF-SEM.
- Mesophyll cells were lobed where chloroplasts were located, facilitating cell-to-cell connections while allowing for greater intercellular airspace exposure. Bundle sheath cells were cylindrical with chloroplasts arranged centrifugally. Chloroplasts occupied *c.* 30–50% of mesophyll cell volume, and 60–70% of bundle sheath cell volume. Roughly 2–3% of each cell surface area was covered by plasmodesmata pit fields for both bundle sheath and mesophyll cells.
- This work will aid future research to develop SBF-SEM methodologies with the aim to better understand the effect of cell structure on C_4 photosynthesis.

Introduction

Photosynthesis research has often depended on microscopic observations. Some examples being the discovery of chloroplasts and their thylakoid structures (reviewed by Staehelin & Paolillo, 2020), or CO_2 diffusion paths including stomata and intercellular airspace (Blackman, 1895; Turrell, 1936), or discovery of C_4 photosynthesis and the role of Kranz anatomy (Hatch & Slack, 1966). Recently, three-dimensional (3D) leaf imaging has been highlighted as a current gap in the application of microscopy to photosynthesis research (Khoshravesh *et al.*, 2022). Recent 3D images of leaf cells including chloroplasts, mitochondria, and peroxisomes have been published (Harwood *et al.*, 2020), but these have mostly been limited to species operating C_3 photosynthesis. While there are far fewer C_4 species than C_3, C_4 species are valuable as both a human food source and a bioenergy source (e.g. maize, sorghum, and sugarcane), and for their role in the global carbon cycle accounting for *c.* 23% of total global CO_2 fixation (Still *et al.*, 2003). Hence, there is also much interest in understanding and improving C_4 photosynthetic traits (Leegood, 2013; von Caemmerer & Furbank, 2016; Koester *et al.*, 2021). The lack of 3D leaf images and analysis of C_4 species is an important knowledge gap in photosynthesis research.

C_4 species differ from C_3 species by using a carbon concentrating mechanism where CO_2 is initially fixed into a four-carbon molecule in mesophyll cells and transported to bundle sheath cells where the four-carbon molecule is decarboxylated releasing CO_2 for fixation by Rubisco, the initial carbon fixing enzyme of the C_3 photosynthetic cycle (Leegood, 2002; Furbank, 2016). A three-carbon molecule is then returned to the mesophyll to replenish intermediates of the C_4 cycle. This carbon concentrating mechanism increases the CO_2 concentration around Rubisco well above ambient CO_2 levels, thus minimizing a competing reaction of the Rubisco substrate Ribulose-1,5-bisphosphate (RuBP) with O_2, a reaction also catalyzed by Rubisco. The oxygenation of RuBP accounts for about a third of reactions catalyzed by Rubisco in C_3 species and is thought to be a wasteful and costly process (Walker *et al.*, 2016).

For plants using C_4 photosynthesis, large metabolic pools are thought to be required for diffusion between mesophyll and bundle sheath cells (Leegood, 1985; Stitt & Heldt, 1985). Two factors that may influence metabolic pool size in C_4 plants are chloroplast volume and plasmodesmata area (Leegood, 2013; Stitt & Zhu, 2014; von Caemmerer & Furbank, 2016). Current photosynthesis research is often directed toward ensuring a sustainable supply of food, fiber, and fuel (Zhu *et al.*, 2022), and identifying targets to redesign photosynthesis is a continuing trend (Ort *et al.*, 2015). While it may be possible to genetically manipulate chloroplast volume and plasmodesmata area, basic understandings of their 3D structure have yet to be explored and

has been the subject of recent research efforts (Danila *et al.*, 2016, 2018, 2019; Harwood *et al.*, 2020).

Chloroplasts are subcellular compartments where light is harvested to produce energy and reducing equivalents, and where CO_2 is fixed into organic molecules used for growth in photosynthetic eukaryotes. Because of their importance, there has been much interest in manipulating photosynthetic capacity by altering chloroplast size or structure (Glynn *et al.*, 2007; Ren *et al.*, 2019). Altering chloroplast size has been shown to affect photosynthetic capacity, chloroplast movement in response to fluctuating light, and CO_2 diffusion from the intercellular air space to the site of carboxylation (Austin & Webber, 2005; Weise *et al.*, 2015; Dutta *et al.*, 2017). However, when working on higher plants, analysis is usually limited to 2D estimates and is most often focused on C_3 and not C_4 species (Staehelin, 2003).

In C_4 species, rapid metabolite transfer between bundle sheath and mesophyll cells is critical for the C_4 mechanisms (Hatch, 1987). This rapid exchange of metabolites between the cells is achieved mainly through plasmodesmata, the tubule-like structures passing through the cell walls of adjacent cells, connecting their cytoplasm (Gunning & Robards, 1976; Hatch, 1987). Many plasmodesmata linking bundle sheath and mesophyll cells have been observed in C_4 species, clustered in groups called a pit field, supporting the idea that large metabolite flux between the two cell types is required (Evert *et al.*, 1977; Hattersley & Browning, 1981). While some recent work has been made in quantifying plasmodesmata, the previous efforts have not been made in proportion to the surface area of the cell or included 'bundle sheath-bundle sheath' connections (Danila *et al.*, 2016, 2018, 2019).

Here, we want to establish a base line for chloroplast volume and surface area, as well as plasmodesmata pit field surface area, of C_4 species and their relationship to the larger cell shape for future work where chloroplast and plasmodesmata size is of interest. Previous findings of C_4 anatomical features are based on 2D views or analysis. This may result in poor or biased information; therefore, it is necessary to investigate the 3D geometry of chloroplasts, cells, and their components such as plasmodesmata for improving accuracy of values and understanding of a 'global view' (Théroux-Rancourt *et al.*, 2017; Danila *et al.*, 2018; Harwood *et al.*, 2020). Because C_4 species often have dimorphic chloroplasts between bundle sheath and mesophyll cell types as well as variable plasmodesmata pit field density, as the functionality of the cells is different, it was important to view both bundle sheath and mesophyll traits (Edwards *et al.*, 2001; Mai *et al.*, 2020). Additionally, we compare chloroplast volume and surface area estimates in maize (*Zea mays*) and sugarcane (*Saccharum* spp. Hybrids) using both serial block face scanning electron microscopy (SBF-SEM) and confocal laser scanning microscopy with the Airyscan system (LSM).

Materials and Methods

Plant materials and growth conditions

Maize and sugarcane were selected as they are widely studied and the two most agriculturally important C_4 crop species in the world (FAO, 2022). Maize (*Zea mays* L., cultivar 'B73') seeds were planted in pots (30.16 cm diameter × 27.94 cm deep; Nursery Supplies Inc.). Sugarcane (a hybrid of *Saccharum officinarum* L. × *Saccharum spontaneum* L., cultivar 'CPCL02-0926') was propagated by nodes. All plants were fertilized with granulated fertilizer (Osmocote Plus 13/13/13; The Scotts Co. LLC, Marysville, OH, USA), water-soluble nutrient solution (Peter's Excel 15-5-15; Everris NA Inc., Dublin, OH, USA), and iron chelate supplement (Sprint 330; BASF Corp., Research Triangle Park, NC, USA) once every 4 wk. Plants were grown in the glasshouse, with temperatures of *c.* 27°C (day) and *c.* 16°C (night), 14-h day length, high-pressure sodium lamps provided an additional 400 μmol m^{-2} s^{-1} photosynthetic photon flux density at canopy level. Plants were rotated every week. For maize, the youngest fully expanded leaves from three plants were selected when plants were 4 wk old. For sugarcane, samples were collected from the youngest fully expanded leaves of three 12-wk-old plants. Leaf samples were taken midway along the leaves, avoiding the large mid-vein. For sugarcane this was *c.* 40 cm from the leaf tip, while for maize it was *c.* 10 cm from the tip.

Sample preparation for SBF-SEM

Leaf samples were prepared following the methodology of Deerinck *et al.* (2010, 2018). Briefly, the 5 × 5 mm samples were immersed in 0.15 M cacodylate buffer (Ted Pella Inc., Redding, CA, USA) pH 7.4 containing 2.5% glutaraldehyde (Electron Microscopy Sciences, Hartfield, PA, USA) and 2.5% paraformaldehyde (Electron Microscopy Sciences) with 2 mM calcium chloride at 35°C for 5 min, placed on ice and fixed for 2 h, washed three times for 5 min each in 0.15 M cacodylate buffer (Ted Pella Inc.) pH 7.4 containing 2 mM calcium chloride, post-fixed in 3% potassium ferrocyanide in 0.3 M cacodylate buffer with 4 mM calcium chloride and 4% aqueous osmium tetroxide (EMS) for 1 h under dark conditions, washed three times in Milli-Q H_2O for 5 min, treated with 1% thiocarbohydrazide (TCH) solution for 20 min, and then washed three times in Milli-Q H_2O for 5 min, immersed in 2% osmium tetroxide (OsT) for 30 min, washed three times in Milli-Q H_2O for 5 min, incubated in 1% uranyl acetate at 4°C for 24 h, washed three times in Milli-Q H_2O for 5 min, transferred into Walton's lead aspartate en bloc staining solution for 30 min at 60°C, washed three times in Milli-Q H_2O for 5 min, dehydrated using ice-cold ethanol solutions of prepared 20%, 50%, 70%, 90%, and 100% for 30 min at each concentration, placed in ice-cold anhydrous acetone for 10 min, transferred into room temperature anhydrous acetone for 10 min, treated for 2 h each at 25% Durcupan™ ACM resin (Sigma-Aldrich) in acetone, 50%, 75%, and 100% for 24 h, mounted between liquid release agent-coated glass slides (EMS) in 100% Durcupan™ ACM resin and put at 60°C for 48 h, released from slides and placed in a template with 100% Durcupan™ ACM resin for 48 h at 60°C.

Sample mounting and SBF-SEM imaging

Epoxy-embedded samples were mounted to aluminum pins (Gatan Inc., Pleasanton, CA, USA) using silver epoxy (Ted Pella)

and sputter coated with a thin layer of Au/Pd prior to block-face imaging. Serial block-face imaging was accomplished using a Sigma VP (Zeiss) equipped with a Gatan 3 View system (model: 3View2XP) and a nitrogen gas injection manifold (Zeiss model 346 061-9002-200). For this work, samples were imaged at 2.0 keV, using 50-nm cutting intervals, 1.0 nm pixel size (12 k × 12 k pixels), beam dwell time of 1.0 µs and a high vacuum chamber pressure of *c.* 5×10^{-3} mbar. Following this method, *c.* 500 images were collected per sample.

Sample preparation and measurements using LSM

Sample preparation for LSM was conducted using a procedure slightly modified from Pignon *et al.* (2019). Leaf samples were cut in 5 mm × 5 mm sections, immediately immersed in water-soluble glycols and resins (Tissue-Tek O.C.T. Compound; Sakura Finetek Inc., Torrance, CA, USA) with a vinyl specimen cryomold (10 mm × 10 mm × 5 mm, Tissue-Tek Cryomold; Sakura Finetek), placed on dry ice to solidify. Cross sections of leaf samples were cut in 10-µm pieces by using a cryostat (Leica CM3050 S; Leica Biosystems, Wetzlar, Germany), placed on glass slides, treated with a membrane and cell wall fluorescent dye solution (FM 1-43FX; Thermo Fisher Scientific, Waltham, MA, USA) for 10 min, which was wiped off, and treated with perfluorodecalin (Sigma-Aldrich) to enhance confocal microscopy depth of penetration (Littlejohn *et al.*, 2010). Sample imaging was performed on a confocal laser scanning microscope with Airyscan system (LSM 880 Airyscan; Carl Zeiss AG) with a × 40 oil-immersion objective (×40 Plan-Apochromat; Carl Zeiss AG). The cell wall staining was excited with the 488-nm laser, and chlorophyll was excited with the 633-nm laser. Serial optical sections were obtained at 1-µm-depth intervals (*z*-stack).

Image processing and analysis

Images obtained by SBF-SEM were aligned using the Gatan Microscopy Suite 3 software (Gatan). After alignment, Amira 9.3 software (Thermo Fisher Scientific) was used to perform segmentation by manually tracing regions of interest (i.e. bundle sheath chloroplasts, plasmodesmata pit field area, and cell walls; Supporting Information Fig. S1) except for mesophyll chloroplasts where the software worked well enough to select individual chloroplasts through multiple *z*-slices. The mesophyll chloroplasts edges were manually cleaned as needed.

Plasmodesmata appear as a tubule penetrating the cell walls of two adjacent cells often in a circular cluster, or pit field, containing many individual plasmodesmata (Fig. S2). The resolution of our images was too low to measure individual plasmodesmata (Fig. S3), so only pit field area was determined. The size of a pit field was calculated as a 2D area on the surface of the cell wall using the software. We divided plasmodesmata into three groups: 'bundle sheath-bundle sheath', 'bundle sheath-mesophyll', and 'mesophyll-mesophyll'. While mesophyll connections to the epidermal layer and bundle sheath connections to the vasculature existed, they were not quantified in this study.

For SBF-SEM, only entire chloroplasts were analyzed for volume (µm^3) and surface area (µm^2). Fifteen bundle sheath chloroplasts and 98 mesophyll chloroplasts across three leaf samples of maize were analyzed, while 19 bundle sheath chloroplasts and 242 mesophyll chloroplasts across three leaf samples of sugarcane were analyzed. Because the software could identify individual mesophyll chloroplasts relatively well, but not bundle sheath chloroplasts, it took approximately the same amount of time to trace the smaller number of bundle sheath chloroplasts as it did the many mesophyll chloroplasts reported here. For estimating cell volume, three bundle sheath cells and six mesophyll cells across three leaf samples of each maize and sugarcane were analyzed. To determine whether shrinkage occurred during sample processing, the diameter of sugarcane bundle sheath cells was measured for both LSM and SBF-SEM images.

Images obtained from LSM were analyzed by using Imaris 9.7 software (BitPlane Inc., Zürich, Switzerland). The Imaris 9.7 software automatically identified unique fluorescent objects from 633 nm excitation (used for chlorophyll autofluorescence), which removed the need for manual tracing; however, identified objects were not always entire chloroplasts or single chloroplasts. This likely led to under- and overestimates of chloroplast volume. From LSM, 573 maize mesophyll chloroplasts and 285 sugarcane mesophyll chloroplasts were analyzed.

To compare shapes (i.e. compare volume and surface area measurements) of chloroplasts imaged by SBF-SEM, we chose to present the data relative to two shapes, a triaxial ellipsoid and a sphere. The volume of a sphere was calculated as

$$\text{Volume} = \frac{4}{3}\pi r^3,$$

where π is the ratio of any circle's circumference to its diameter ($\pi \approx 3.14159$) and r is the radius, or length from the center of the circle to the perimeter. The surface area of the sphere was calculated as

$$\text{Surface area} = 4\pi r^2.$$

The volume of the ellipsoid was calculated as

$$\text{Volume} = \frac{4}{3}\pi(a\ b\ c),$$

where a, b, and c are the three lengths from the center of the ellipsoid to the perimeter along each axis. The surface area of the ellipsoid was estimated as

$$\text{Surface area} \approx 4\pi \sqrt[p]{\frac{a^p b^p + a^p c^p + b^p c^p}{3}},$$

where $p \approx 1.6075$ (Klamkin, 1971; Xu *et al.*, 2009). The values of b and c were held constant relative to a such that $a = 2b = 6c$; for comparison in a sphere $a = b = c$. This relationship between a, b, and c was not empirically derived or fit but was initially approximated by viewing chloroplast images and settled on after

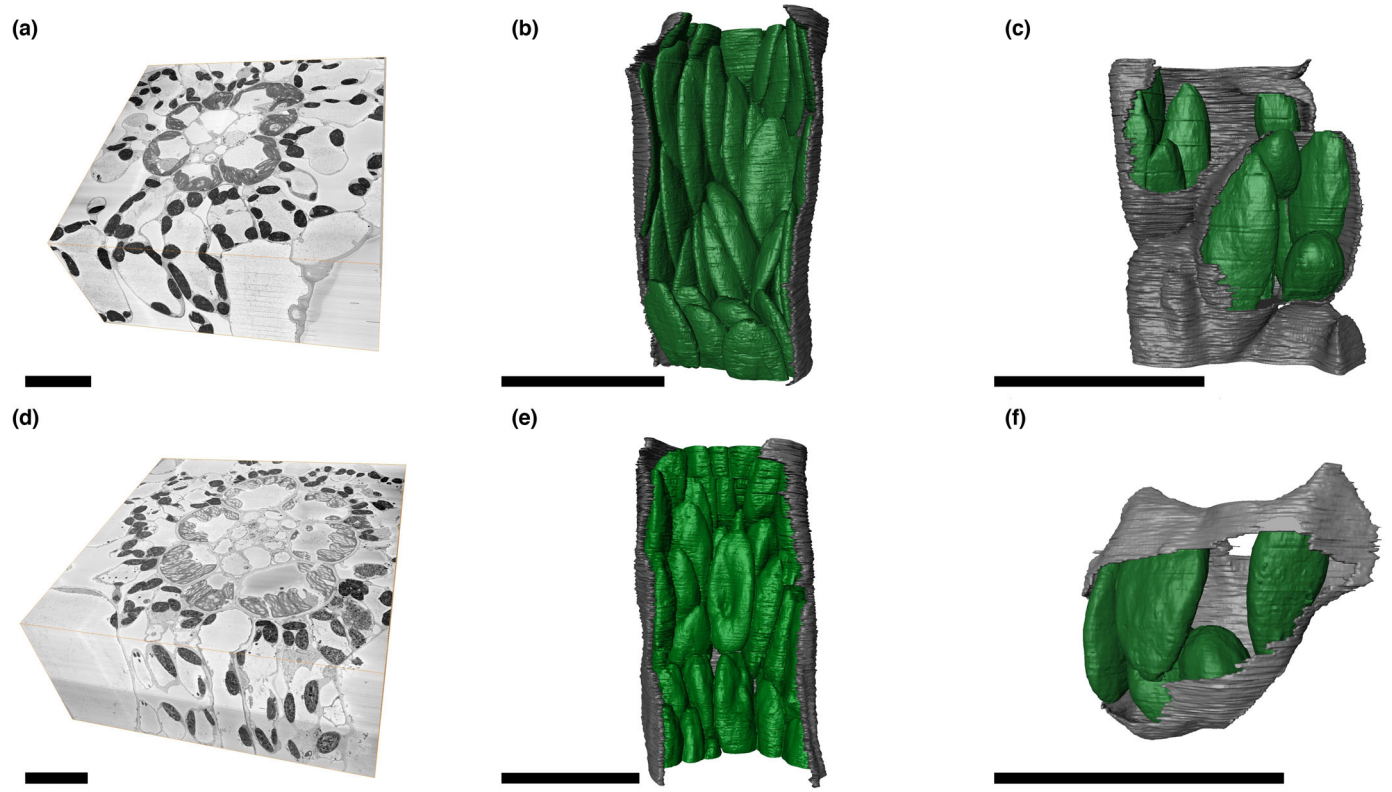

Fig. 1 Examples of maize (a–c) and sugarcane (d–f) images obtained from serial block face scanning electron microscopy (SBF-SEM) to calculate chloroplast parameters. 3D image block of a leaf cross section comprised of *c.* 500 images (a, d). 3D visualization of a portion of a single bundle sheath cell with chloroplasts (b, e). 3D visualization of a portion of a mesophyll cell with chloroplasts (c, f). Bars, 10 μm.

Table 1 Volume and surface area of maize and sugarcane chloroplasts obtained from serial block face scanning electron microscopy (SBF-SEM) measurements.

	Volume (μm^3)			Surface area (μm^2)		
Type	Mean	Minimum	Maximum	Mean	Minimum	Maximum
Maize						
Bundle sheath	40.5 ± 2.7	27.7	51.9	100.1 ± 5.7	76.1	126.5
Mesophyll	20.1 ± 0.7	8.7	37.6	52.4 ± 1.5	23.8	94.1
Sugarcane						
Bundle sheath	86.2 ± 6.5	55.4	141.1	146.1 ± 11.4	97.0	252.4
Mesophyll	30.3 ± 0.8	13.4	52.6	73.3 ± 2.0	41.9	127.5

Data are means ± SE.

comparisons of volume to surface area plots of chloroplasts. For plots of volume-to-surface area, the values of a for both the sphere and the ellipsoid were allowed to vary such that the resulting volumes included the range of measured chloroplasts. Calculations and plots were made in Excel for Microsoft Office 365 (Microsoft, Redmond, WA, USA). An example of the two shapes is also presented and was made in Matlab (MathWorks, Natick, MA, USA).

Statistical analysis

Bundle sheath and mesophyll chloroplast volume determined by SBF-SEM were compared by t-test using PROC TTEST procedure in Sas within species (SAS Institute Inc., Cary, CA, USA).

Results

SBF-SEM estimates of chloroplast volume and surface area

Bundle sheath and mesophyll chloroplasts of three maize and three sugarcane plants were reconstructed based on SBF-SEM images (Fig. 1; Table 1). Both maize and sugarcane had predominantly triaxial ellipsoid shaped chloroplasts in both the bundle sheath and mesophyll cells (Figs 1, 2). The volume of individual bundle sheath chloroplasts was approximately two- to threefold larger than mesophyll chloroplasts (maize $P = 0.01$, sugarcane $P = 0.03$; Figs 2, S4; Table 1). The bundle sheath chloroplast surface area to volume ratio was *c.* 3 m^2 m^{-3} in maize and *c.* 2 m^2 m^{-3} in sugarcane, and the

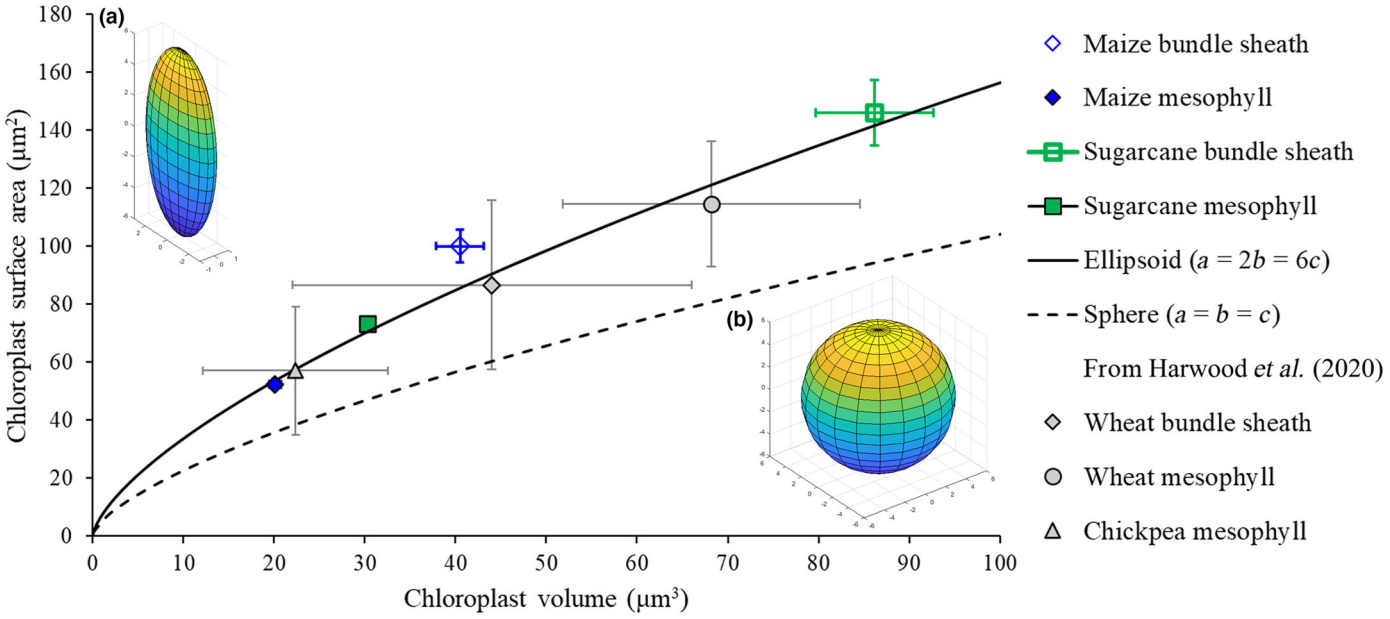

Fig. 2 Plot of chloroplast volume to surface area determined by serial block face scanning electron microscopy (SBF-SEM) for maize and sugarcane compared with previously published values. Symbols are the mean for each species cell type with error bars showing ±SE. Solid line shows the volume–surface area of a triaxial ellipsoid. The dotted line shows the volume–surface area relationship of a sphere. Insets: (a) the example of ellipsoid shape ($a = 2b = 6c$), and (b) the example of sphere shape ($a = b = c$).

mesophyll chloroplast surface area-to-volume ratio was *c.* 3 $m^2\ m^{-3}$ in both species. It should be noted that the ratio of surface area to volume is not constant (Fig. 2).

LSM estimates of chloroplast volume and surface area

Laser scanning microscopy was used to estimate chloroplast volume to compare with SBF-SEM. Tight packing of bundle sheath chloroplasts made distinguishing individual chloroplasts difficult; therefore, only mesophyll chloroplast volume was compared for these measurements (Fig. 3). The chloroplast volume estimated by LSM was more variable and larger than that determined by the SBF-SEM method (Fig. 4). The mean mesophyll chloroplast volume in maize was 56.7 μm^3 when measured using LSM, ranging from 3.4 to 593.7 μm^3 (Fig. 4; Table S1). The mesophyll chloroplast volume in sugarcane was 197.3 μm^3 on average, varying from 3.2 to 1652.5 μm^3 (Fig. 4; Table S1). Given these wide volume ranges, a subset of the chloroplast data is also presented based on the expected sizes determined by SBF-SEM (Fig. 4). Shrinkage appears to be possible during SBF-SEM sample preparation when compared to LSM. The mean diameter of sugarcane bundle sheath cells determined by SBF-SEM was 0.664 times smaller than the mean from LSM images (15.0 μm compared to 22.6 μm; Fig. S5). To correct for the upper limit of what is considered a reasonable size of chloroplast in the LSM images, we divided the largest measured chloroplast in the SBF-SEM data set by 0.29 (i.e. 0.664^3, assuming equal shrinkage occurred in three dimensions). This determined the upper limit of chloroplast volume to be 130 μm^3 in maize and 181 μm^3 in sugarcane for the LSM subset (Fig. 4).

SBF-SEM estimates of bundle sheath and mesophyll cell properties

Bundle sheath cells showed a cylinder shape tapering off to one side at the top and the bottom where two bundle sheath cells were connected forming a column (Figs 1, 5, 6, S6). Bundle sheath chloroplasts were mostly distributed in a centrifugal position (located near mesophyll cells and away from vasculature). Mesophyll cells had an atypical geometry, appearing to have a central shaft with protruding lobes along the length. Lobes were often filled with chloroplast and facilitated connections to neighboring cells via plasmodesmata (Figs 1, 5). For size estimates, there is the possibility of shrinkage during processing (Khoshravesh *et al.*, 2022). Here, bundle sheath cell diameters were *c.* 0.66 times smaller in SBF-SEM than LSM images (Fig. S5).

Due to the sampling depth of our images, we were not able to view entire cells. The average observed volume of a maize bundle sheath and mesophyll cell was *c.* 1600 μm^3 (Table 2). In this observable portion of maize cells, *c.* 25 chloroplasts were observed per bundle sheath and mesophyll cell. On a volume-to-volume comparison, 70.8% of the observed bundle sheath volume was occupied by chloroplasts and 33.1% of observed mesophyll volume was occupied by chloroplasts (Table 2). For sugarcane, the average observable volume of a bundle sheath cell was *c.* 3000, and *c.* 1000 μm^3 for a mesophyll cell (Table 2). The average number of chloroplasts per observable cell volume was *c.* 20 in both bundle sheath and mesophyll cell types (Table 2). For sugarcane, we estimate that 60.2% of bundle sheath cell volume is occupied by chloroplasts and 49.6% of mesophyll cell volume is occupied by chloroplasts. Bundle sheath and mesophyll cell wall thickness were similar in maize. Sugarcane bundle sheath cells had much thicker cell walls than the mesophyll cells (Table 3).

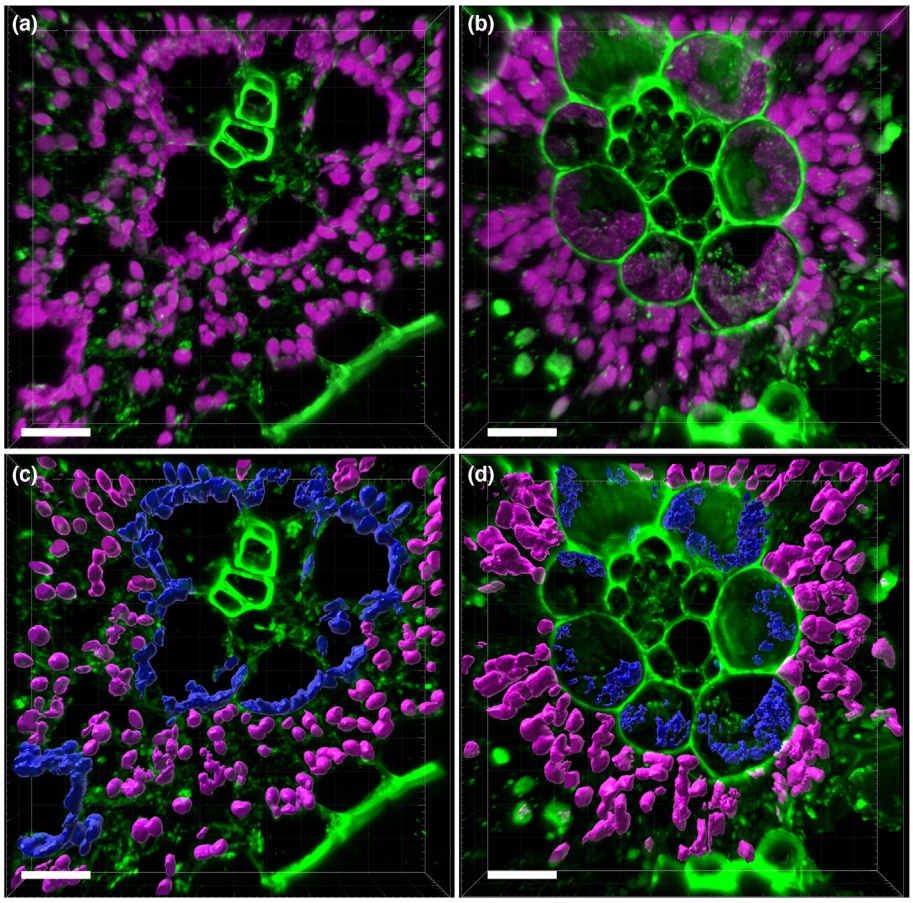

Fig. 3 Leaf cross sections obtained from confocal laser scanning microscopy with the Airyscan system (LSM). Upper panels show maize (a) and sugarcane (b) leaf cross section images with chloroplasts (magenta) and cell wall (green). Lower panels show the 3D visualization of maize (c) and sugarcane (d) bundle sheath chloroplasts (blue) and mesophyll chloroplasts (magenta). Bars, 20 μm.

SBF-SEM estimates of plasmodesmata pit field area

For the portion of cells observed here, one bundle sheath cell would connect laterally to two other bundle sheath cells and three to five mesophyll cells. As bundle sheath cells are also connected end to end (Fig. S6), it is assumed that each bundle sheath cell is connected to four other bundle sheath cells in total. A single mesophyll cell was observed to connect to one or two bundle sheath cells and two or three other mesophyll cells. As the entire cell was not observed, these estimates of cellular connections are likely low.

In maize, plasmodesmata pit field area of 'bundle sheath-bundle sheath' connections was 1.0% of the observed bundle sheath cell surface area, 'bundle sheath-mesophyll' connections was 1.9% (Table 3). The pit field area of 'bundle sheath-mesophyll' connections was 0.9% of the mesophyll cell surface area, 'mesophyll-mesophyll' was 1.2% (Table 3). Overall, 3% of maize bundle sheath surface area was covered in plasmodesmata pit fields and 2.2% of mesophyll cells were covered in plasmodesmata pit fields. In sugarcane, the total area of the cell covered in plasmodesmata was 3%, the same as was observed in maize (Table 3). However, sugarcane appeared to have more 'bundle sheath-mesophyll' pit fields and fewer 'bundle sheath-bundle sheath' pit fields compared with maize (Fig. 6; Table S2). Despite sugarcane having larger bundle sheath cells than maize, this resulted in a larger percentage of plasmodesmata pit field coverage of 'bundle sheath-mesophyll' connections at 2.7% of the bundle sheath cell surface area compared to the 1.9% observed in maize. Only 0.3% of the sugarcane bundle sheath surface contained 'bundle sheath-bundle sheath' pit fields compared to 1.0% in maize. The area and percent coverage of plasmodesmata pit fields for sugarcane mesophyll cells was similar to maize (Table 3).

Discussion

Trade-offs between SBF-SEM and LSM for determining chloroplast size and shape

Studies that have looked at chloroplast size of C_4 species used light microscopy, confocal laser scanning microscopy, and transmission electron microscopy, but the ability to identify the volume of single chloroplast was limited (Stata *et al.*, 2014; Pignon *et al.*, 2019; Maai *et al.*, 2020). Additionally, variability between studies can be large. For example, chloroplast length of sugarcane has been reported as low as 4.83 μm while maize has been reported as high as 43.14 μm (Du *et al.*, 2019; Zhang *et al.*, 2021). Recently, SBF-SEM was proposed as a better method for determining chloroplast volume, as Harwood *et al.* (2020) showed extrapolating volume from 2D images, like those from light microscopy or transmission electron microscopy, was inaccurate. However, the Harwood's study was limited to C_3 species.

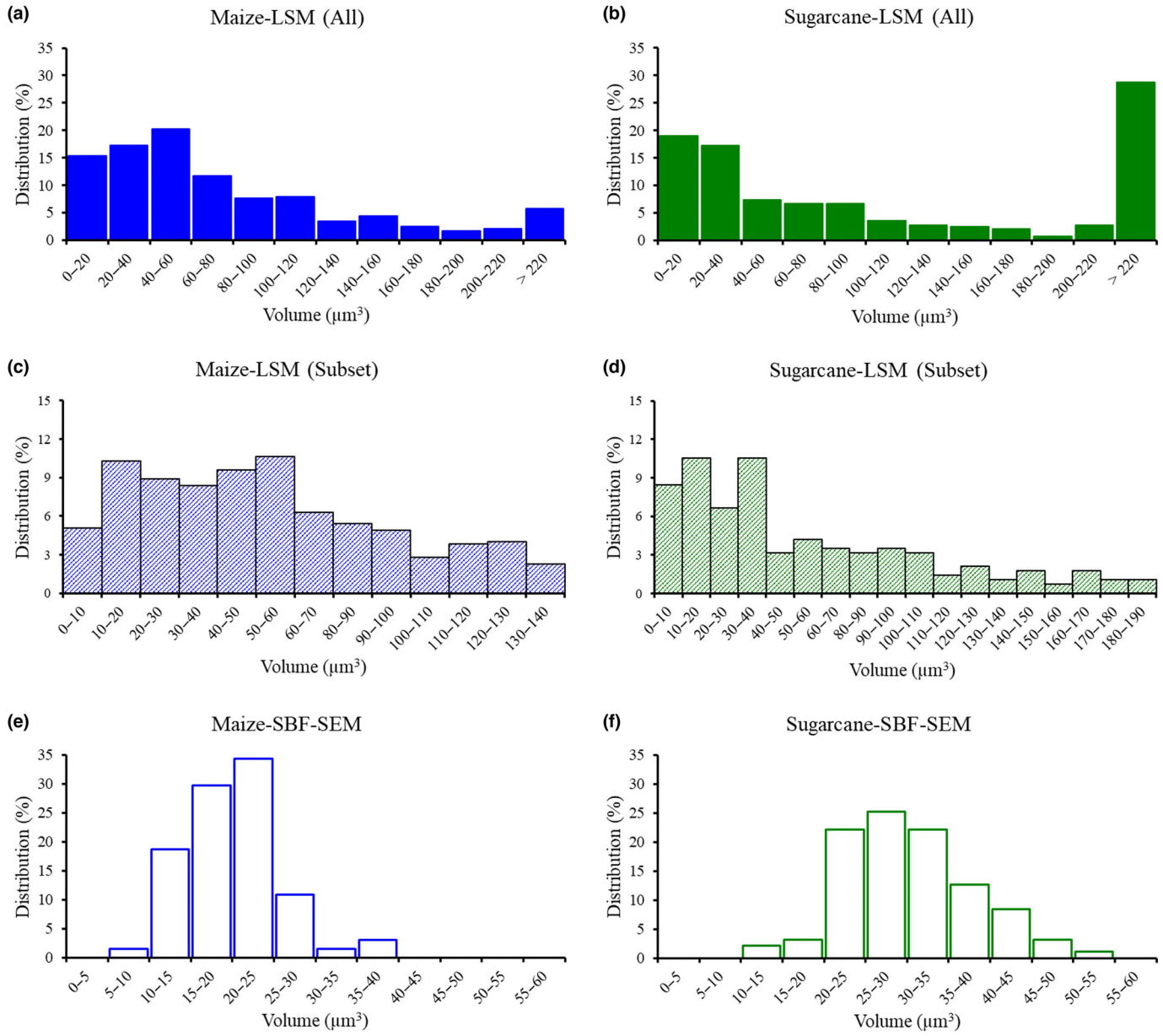

Fig. 4 Histograms of mesophyll chloroplast volume distributions in maize (blue bars; a, c, e) and sugarcane (green bars; b, d, f) comparing two microscopy methods. Upper panels (closed bars; a, b, c, d) show mesophyll chloroplast volume measured by confocal laser scanning microscopy with the Airyscan system (LSM) for all objects identified by the software (a, b), or a subset (c, d) corresponding to expected values from serial block face scanning electron microscopy (SBF-SEM) corrected for possible shrinkage during sample preparation. Lower panels (open bars; e, f) show mesophyll chloroplast volume measured by SBF-SEM.

In this experiment, we tested two different microscopy methods, SBF-SEM and LSM, for estimating chloroplasts volume of two C_4 species, maize and sugarcane. SBF-SEM showed clear images of chloroplasts but was time- and labor-intensive. Additionally, shrinkage of the sample during SBF-SEM preparation may occur and should be considered (Fig. S5; Khoshravesh *et al.*, 2022). LSM method had easy sample preparation, quick image acquisition and analysis. However, it was not able to differentiate individual chloroplasts if they were tightly packed. This was because the software merged multiple chloroplasts into a single object during 3D reconstruction, which led to large variation of chloroplast parameters when using LSM. Even when cutoffs were used to exclude erroneously low and high volumes, it was unclear that a reasonable distribution of individual chloroplasts volumes was observed. Pignon *et al.* (2019) used the same LSM method to determine total chloroplast volume per unit leaf area. We suggest that while this LSM method is suitable for total chloroplast volume, it does not suitably measure individual chloroplast volumes.

Chloroplast and cell comparisons

In many 2D analyses of C_4 species, mesophyll chloroplasts are reported to be smaller than bundle sheath chloroplasts (Black Jr

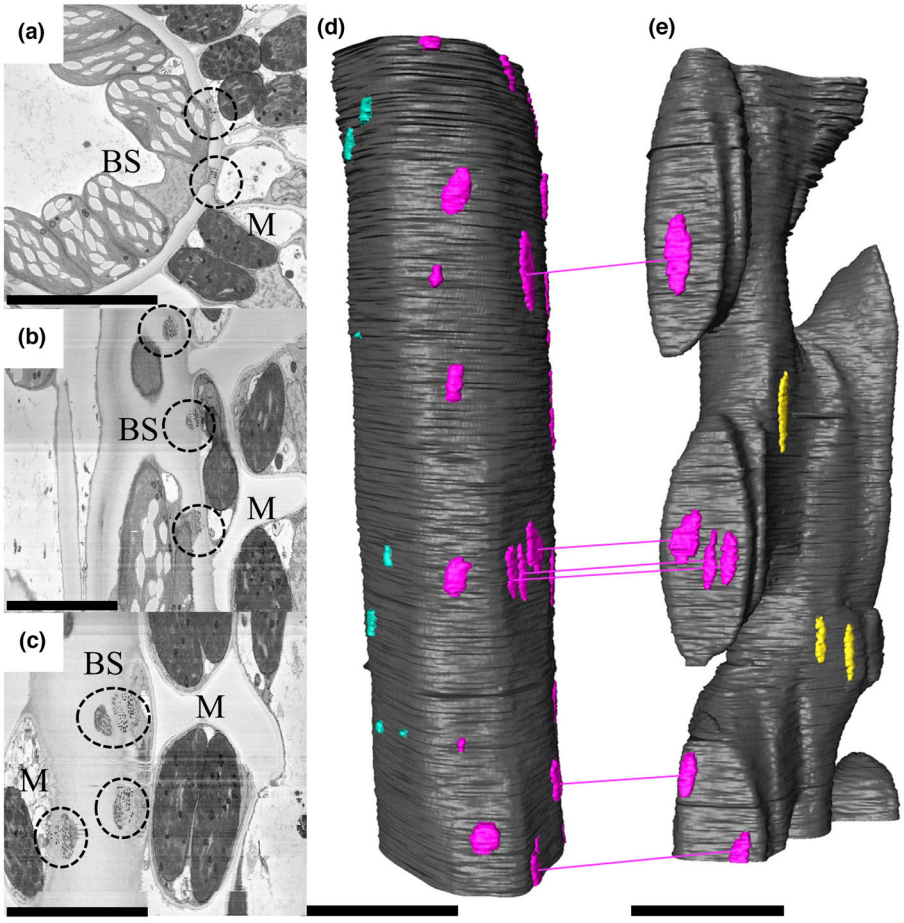

Fig. 5 Example of 2D images and 3D visualizations of bundle sheath and mesophyll cell wall with plasmodesmata pit fields in a sugarcane leaf sample. Panels (a–c) show 2D images of plasmodesmata between bundle sheath and mesophyll cells from the *xy*-view (a), the *yz*-view (b), and the *xz*-view (c). Black dotted circles indicate plasmodesmata connecting 'bundle sheath-mesophyll' in a 2D-view. Panel (d) shows a 3D visualization of bundle sheath with plasmodesmata pit fields, and (e) shows a 3D visualization of a mesophyll cell with plasmodesmata pit fields. For (d, e), grey color indicates cell walls, cyan color shows plasmodesmata pit field area between 'bundle sheath-bundle sheath', magenta color shows plasmodesmata pit field area between 'bundle sheath-mesophyll', and yellow shows plasmodesmata pit field area between 'mesophyll-mesophyll'. Magenta lines indicate which pit fields connected the bundle sheath and mesophyll cells shown. BS, bundle sheath cell; M, mesophyll cell. Bars, 5 μm.

& Mollenhauer, 1971; Liu & Dengler, 1994; Muhaidat *et al.*, 2011). Our results in maize and sugarcane support the generalization of chloroplast size, with mesophyll chloroplast volume being *c.* 35–50% smaller than those in the bundle sheath. When compared to SBF-SEM data from Harwood *et al.* (2020), the mesophyll chloroplast volume of maize and sugarcane in this experiment was smaller than wheat but comparable to chickpea (Fig. 2). Additionally, the maize and sugarcane volume-to-surface area relationship observed here is similar to the measurements of wheat and chickpea performed by Harwood *et al.* (2020) when a triaxial ellipsoid with semi-axial lengths of $a = 2b = 6c$ is assumed (Fig. 2). This approximates the chloroplast shape, but as Harwood *et al.* (2020) noted chloroplasts are better described as flattened ovoid concaved disks.

C_4 species are sometimes reported to have fewer mesophyll chloroplasts per cell than bundle sheath chloroplasts perhaps to allow adequate light penetration to bundle sheath cells (Black Jr & Mollenhauer, 1971; Liu & Dengler, 1994; Muhaidat *et al.*, 2011). Our estimates of chloroplasts per cell were similar between mesophyll and bundle sheath cells. Unfortunately, the methods used here did not allow us to capture entire mesophyll or bundle sheath cells and limited the number of cells that could be analyzed. Using estimates for the length of cells from other sources (Table S3; Fig. S7) and the count of chloroplasts per cell observed in our SBS-SEM images, we estimate maize has 53 chloroplasts in both cell types, and sugarcane has 49 chloroplasts per mesophyll cell and 62 chloroplasts per bundle sheath cell. Given the approximate nature of these estimates, and that bundle sheath cell volume is understood to vary considerably, we cannot confirm mesophyll cells contain fewer chloroplasts than bundle sheath cells. Additionally, our estimates for the volume of a cell occupied by chloroplasts, up to 70% of bundle sheath cell volume and 50% of mesophyll cell volume, are higher than previously reported. Pignon *et al.* (2019) estimated 8–14% in mesophyll cells and 15–25% in bundle sheath cells in four C_4 species. Similarly, Stata *et al.* (2014) reported that chloroplasts occupy 12% of cell area. These differences may be explained by 2D analysis limitations of previous studies, or by different environmental conditions. For example, light intensity is reported to alter chloroplast number per cell as well as their structure and arrangement (Feng *et al.*, 2019).

Mesophyll chloroplasts were located near plasmodesmata, in the lobbed protrusions that facilitated the cell–cell connections. While it is interesting that mesophyll chloroplasts were adjacent to plasmodesmata possibly facilitating rapid metabolite transport between cells, chloroplast location is likely dynamic as it has been shown that C_4 chloroplast move in response to light and other stimuli (Maai *et al.*, 2011, 2020). Similarly, Danila *et al.* (2016) described the shape of maize mesophyll cells as highly lobed and positioned irregularly with air spaces in between mesophyll cells.

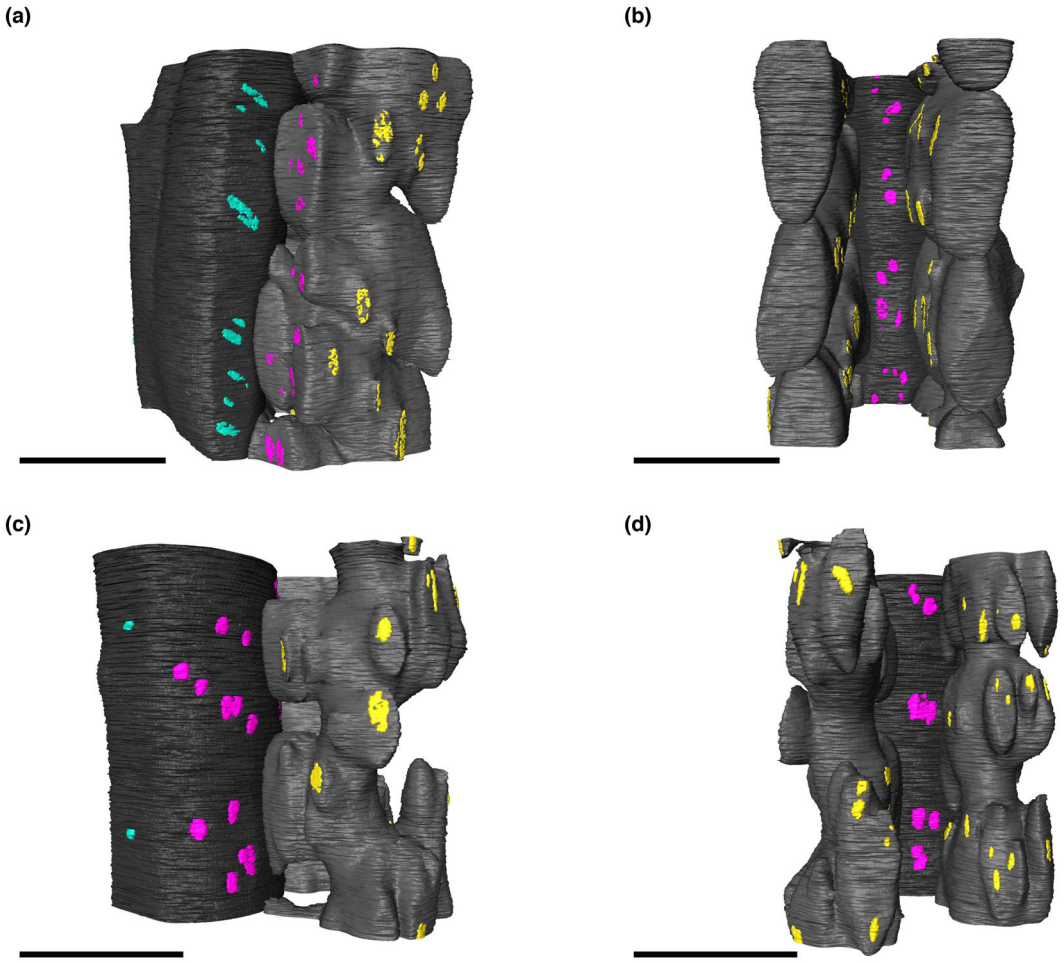

Fig. 6 3D visualization of a bundle sheath and mesophyll cell with plasmodesmata pit fields in maize (a, b) and sugarcane (c, d). Panels (a, c) show the *xz*-view, (b, d) show the *yz*-view. Not all cells in the image were reconstructed for the 3D view in order to show plasmodesmata on the cell surfaces. Grey and dark grey colors indicate mesophyll and bundle sheath cell walls, and cyan color shows plasmodesmata pit field area between 'bundle sheath-bundle sheath', magenta color shows plasmodesmata pit field area between 'bundle sheath-mesophyll', and yellow shows plasmodesmata pit field area between 'mesophyll-mesophyll'. Bars, 10 μm.

Table 2 Maize and sugarcane bundle sheath and mesophyll cell parameters obtained from the serial block face scanning electron microscopy (SBF-SEM) measurements (entire cells were not observed).

Type	Observable volume of cell (μm^3)	Observable surface area of cell (μm^2)	Chloroplast count in observed volume	Chloroplast volume in observed volume (μm^3)	Cell volume occupied by chloroplast (%)
Maize					
Bundle sheath	1603.2 ± 496.3	1180.4 ± 196.2	25.7 ± 5.8	1010.5 ± 103.4	70.8 ± 13.5
Mesophyll	1627.4 ± 240.9	1557.5 ± 180.6	26.2 ± 3.5	533.2 ± 121.9	33.1 ± 2.8
Sugarcane					
Bundle sheath	3177.0 ± 936.4	1987.4 ± 358.6	23.0 ± 7.0	1778.9 ± 358.6	60.2 ± 7.6
Mesophyll	1158.9 ± 156.4	1295.5 ± 161.5	18.3 ± 1.4	543.5 ± 121.9	49.6 ± 4.0

Data are means ± SE.

It is possible that our observed mesophyll cell shape was distorted by the sample preparation for SBF-SEM (Khoshravesh *et al.*, 2022); however, Danila *et al.* (2016) used different methods. This mesophyll cell shape is likely functionally important. The protruding lobes form cell–cell connections and the thinner cell diameters between the lobes allows for intercellular airspace, which is necessary for CO_2 diffusion within the leaf mesophyll.

Being able to capture entire cell volumes is important for accurate characterization of these traits. Here, we used a slice depth of 0.05 μm over 500 slices, for a total of 25 μm, which failed to

Table 3 Sum of all plasmodesmata pit field areas per observable portions of cell in maize and sugarcane, for both bundle sheath and mesophyll cells obtained from serial block face scanning electron microscopy (SBF-SEM) images (entire cells were not observed).

	Species	
Parameter	Maize	Sugarcane
Bundle sheath cell		
Cell wall thickness (μm)	0.1 ± 0.0	0.6 ± 0.0
BS–BS PF area per observed portion of BS (μm^2)	11.5 ± 1.8	6.0 ± 1.1
BS–BS PF area per BS surface area (%)	1.0 ± 0.1	0.3 ± 0.1
BS–M PF area per observed portion of BS (μm^2)	25.3 ± 9.3	51.6 ± 4.8
BS–M PF area per BS surface area (%)	1.9 ± 0.5	2.7 ± 0.3
Total PF area per observed portion of BS (μm^2)	36.8 ± 10.8	57.6 ± 4.9
Total PF area per BS surface area (%)	3.0 ± 0.4	3.0 ± 0.4
Mesophyll cell		
Cell wall thickness (μm)	0.1 ± 0.0	0.1 ± 0.0
M–BS PF area per observed portion of M (μm^2)	14.5 ± 2.8	15.0 ± 1.7
M–BS PF area per M surface area (%)	0.9 ± 0.1	1.2 ± 0.1
M–M PF area per observed portion of M (μm^2)	19.8 ± 3.0	16.8 ± 2.9
M–M PF area per M surface area (%)	1.2 ± 0.1	1.3 ± 0.1
Total PF area per observed portion of M (μm^2)	34.4 ± 5.6	31.9 ± 3.4
Total PF area per M surface area (%)	2.2 ± 0.2	2.5 ± 0.1

Data are means ± SE. BS, bundle sheath; BS–BS, bundle sheath–bundle sheath cell interface; BS–M, bundle sheath–mesophyll cell interface; M, mesophyll; M–BS, mesophyll–bundle sheath cell interface; M–M, mesophyll–mesophyll cell interface; PF, plasmodesmata pit field.

capture an entire cell length. Cells are expected to be *c.* 50 μm long (Danila *et al.*, 2018). Increasing the slice depth to 0.1 μm may capture entire cells but would limit analysis of smaller cell structures. Switching to a paradermal, rather than a cross-sectional view, and decreasing resolution may also allow for capture of entire cells.

Plasmodesmata comparisons

Plasmodesmata are critical for metabolite transport between cells, especially for the coordination of the C_3 and C_4 photosynthetic cycles that are spatially separated between bundle sheath and mesophyll cells in most C_4 species. Previous attempts to quantify plasmodesmata or related traits were based on transmission electron microscopy (Gunning, 1978; Seagull, 1983; Botha, 1992), and recently, Danila *et al.* (2016, 2018, 2019) developed a method to combine 3D immunolocalization confocal microscopy with scanning electron microscope. In this experiment, we investigated plasmodesmata pit field area in maize and sugarcane using SBF-SEM to understand how plasmodesmata area is three-dimensionally distributed in bundle sheath and mesophyll cells. While previous research has mainly focused on plasmodesmata 'bundle sheath-mesophyll' connections, we reported here that different patterns of plasmodesmata pit fields between 'bundle sheath-bundle sheath', 'bundle sheath-mesophyll', and 'mesophyll-mesophyll' may occur in a species-dependent manner.

Maize devoted about threefold more cell surface area to 'bundle sheath-bundle sheath' plasmodesmata connection than sugarcane on a percentage basis (1% compared to 0.3%), and about a third less surface area than sugarcane to 'bundle sheath-mesophyll' connections on a percentage basis (1.8% compared to 2.7%). Even though interpretation is limited when comparing only two species, our observations could suggest more metabolite sharing among bundle sheath cells in maize than in sugarcane. Danila *et al.* (2018) found that 'bundle sheath-mesophyll' plasmodesmata area is different depending on C_4 biochemical subtype. In the two species we investigated, maize operates both NADP-ME and PEPCK pathways, while sugarcane operates only the NADP-ME pathway (Wingler *et al.*, 1999).

When modeling photosynthesis, plasmodesmata parameterization can be useful. For example, Jenkins *et al.* (1989) estimated that 60% of CO_2 leakage takes place through plasmodesmata. Wang *et al.* (2014) used the length of the plasmodesmata pathway, the 'bundle sheath–mesophyll' cell interface per unit leaf area, the surface fraction of plasmodesmata, and the diffusion coefficient for the given metabolite to calculate the rate of metabolite movement through plasmodesmata. Here, we presented pit field area, as we were not able to consistently trace individual plasmodesmata tubules between cells. Danila *et al.* (2016, 2018, 2019) has been able to identify plasmodesmata density within pit fields and this could be used to estimate plasmodesmata area from the pit field area presented here, but ideally plasmodesmata density should be determined within the same study. For SBF-SEM, plasmodesmata traces may be lost between *z*-slices as the diameter of a typical plasmodesmata is likely < 25 nm (Yan *et al.*, 2019). By decreasing slice depth and increasing resolution, we may be able to more accurately trace individual plasmodesmata.

Conclusion

Here, we showed that LSM was unable to differentiate individual chloroplast volumes in C_4 leaf tissue. Individual chloroplast volumes could be determined with SBF-SEM, but required large time and labor investments, and sample shrinkage may distort size estimates. Plasmodesmata pit fields were clearly visible in the SBF-SEM images; however, more work is needed to capture entire cells and individual plasmodesmata. This work represents one of the first 3D reconstructions of C_4 chloroplasts and cell structures, advancing SBF-SEM methodologies with the aim to better understand how cellular structures effect photosynthetic performance.

Acknowledgements

The information, data, or work presented herein was funded in part by the Biological and Environmental Research (BER) program, US Department of Energy, under Award Number DE-SC0018254. The views and opinions of authors expressed hereicn do not necessarily state or reflect those of the US Government or any agency thereof.

Competing interests

None declared.

Author contributions

M-SL and RAB contributed equally to this work. Conceiving and designing the experiments were performed by DRO, M-SL and RAB. M-SL, RAB and KAB were involved in performing the experiments M-SL and RAB analyzed the data. Writing original draft preparation, review, and editing were performed by DRO, M-SL, RAB and KAB.

ORCID

Kingsley A. Boateng https://orcid.org/0000-0002-1974-5905
Ryan A. Boyd https://orcid.org/0000-0003-4009-7700
Moon-Sub Lee https://orcid.org/0000-0003-3849-5611
Donald R. Ort https://orcid.org/0000-0002-5435-4387

Data availability

All data pertinent to this work are included in the article and the Supporting Information.

References

Austin J, Webber AN. 2005. Photosynthesis in *Arabidopsis thaliana* mutants with reduced chloroplast number. *Photosynthesis Research* **85**: 373–384.

Black CC Jr, Mollenhauer HH. 1971. Structure and distribution of chloroplasts and other organelles in leaves with various rates of photosynthesis. *Plant Physiology* **47**: 15–23.

Blackman FF. 1895. XI. Experimental researches on vegetable assimilation and respiration. No. II. On the paths of gaseous exchange between aerial leaves and the atmosphere. *Philosophical Transactions of the Royal Society of London. Series B: Biological Sciences* **186**: 503–562.

Botha CEJ. 1992. Plasmodesmatal distribution, structure and frequency in relation to assimilation in C_3 and C_4 grasses in southern Africa. *Planta* **187**: 348–358.

von Caemmerer S, Furbank RT. 2016. Strategies for improving C_4 photosynthesis. *Current Opinion in Plant Biology* **31**: 125–134.

Danila FR, Quick WP, White RG, Furbank RT, von Caemmerer S. 2016. The metabolite pathway between bundle sheath and mesophyll: quantification of plasmodesmata in leaves of C_3 and C_4 monocots. *Plant Cell* **28**: 1461–1471.

Danila FR, Quick WP, White RG, Kelly S, von Caemmerer S, Furbank RT. 2018. Multiple mechanisms for enhanced plasmodesmata density in disparate subtypes of C_4 grasses. *Journal of Experimental Botany* **69**: 1135–1145.

Danila FR, Quick WP, White RG, von Caemmerer S, Furbank RT. 2019. Response of plasmodesmata formation in leaves of C_4 grasses to growth irradiance. *Plant, Cell & Environment* **42**: 2482–2494.

Deerinck TJ, Bushong EA, Thor A, Ellisman MH. 2010. *NCMIR methods for 3D EM: a new protocol for preparation of biological specimens for serial block face scanning electron microscopy*. National Center for Microscopy and Imaging Research. [WWW document] URL www.ncmir.ucsd.edu/sbem-protocol [accessed 27 December 2021].

Deerinck TJ, Shone TM, Bushong EA, Ramachandra R, Peltier ST, Ellisman MH. 2018. High-performance serial block-face SEM of nonconductive biological samples enabled by focal gas injection-based charge compensation. *Journal of Microscopy* **270**: 142–149.

Du Q, Zhao XH, Xia L, Jiang CJ, Wang XG, Han Y, Wang J, Yu HQ. 2019. Effects of potassium deficiency on photosynthesis, chloroplast ultrastructure, ROS, and antioxidant activities in maize (*Zea mays* L.). *Journal of Integrative Agriculture* **18**: 395–406.

Dutta S, Cruz JA, Imran SM, Chen J, Kramer DM, Osteryoung KW. 2017. Variations in chloroplast movement and chlorophyll fluorescence among chloroplast division mutants under light stress. *Journal of Experimental Botany* **68**: 3541–3555.

Edwards GE, Furbank RT, Hatch MD, Osmond CB. 2001. What does it take to be C_4? Lessons from the evolution of C_4 photosynthesis. *Plant Physiology* **125**: 46–49.

Evert RF, Eschrich W, Heyser W. 1977. Distribution and structure of the plasmodesmata in mesophyll and bundle-sheath cells of *Zea mays* L. *Planta* **136**: 77–89.

FAO. 2022. *World food and agriculture – statistical yearbook 2022*. [WWW document] URL doi: 10.4060/cc2211en [accessed 12 January 2023].

Feng L, Raza MA, Li Z, Chen Y, Khalid MHB, Du J, Liu W, Wu X, Song C, Yu L *et al.* 2019. The influence of light intensity and leaf movement on photosynthesis characteristics and carbon balance of soybean. *Frontiers in Plant Science* **9**: 1952.

Furbank RT. 2016. Walking the C_4 pathway: past, present, and future. *Journal of Experimental Botany* **67**: 4057–4066.

Glynn JM, Miyagishima SY, Yoder DW, Osteryoung KW, Vitha S. 2007. Chloroplast division. *Traffic* **8**: 451–461.

Gunning BES. 1978. Age-related and origin-related control of the numbers of plasmodesmata in cell walls of developing *Azolla* roots. *Planta* **143**: 181–190.

Gunning BES, Robards AW. 1976. *Intercellular communication in plants: studies on plasmodesmata*. New York, NY, USA: Springer-Verlag.

Harwood R, Goodman E, Gudmundsdottir M, Huynh M, Musulin Q, Song M, Barbour MM. 2020. Cell and chloroplast anatomical features are poorly estimated from 2D cross-sections. *New Phytologist* **225**: 2567–2578.

Hatch MD. 1987. C_4 photosynthesis: a unique blend of modified biochemistry, anatomy and ultrastructure. *Biochimica et Biophysica Acta* **895**: 81–106.

Hatch MD, Slack CR. 1966. Photosynthesis by sugar-cane leaves: a new carboxylation reaction and the pathway of sugar formation. *Biochemical Journal* **101**: 103–111.

Hattersley PW, Browning AJ. 1981. Occurrence of the suberized lamella in leaves of grasses of different photosynthetic types. I. In parenchymatous bundle sheaths and PCR ("Kranz") sheaths. *Protoplasma* **109**: 371–401.

Jenkins CL, Furbank RT, Hatch MD. 1989. Mechanism of C_4 photosynthesis: a model describing the inorganic carbon pool in bundle sheath cells. *Plant Physiology* **91**: 1372–1381.

Khoshravesh R, Hoffmann N, Hanson DT. 2022. Leaf microscopy applications in photosynthesis research: identifying the gaps. *Journal of Experimental Botany* **73**: 1868–1893.

Klamkin M. 1971. Elementary approximations to the area of *N*-dimensional ellipsoids. *The American Mathematical Monthly* **78**: 280–283.

Koester RP, Pignon CP, Kesler DC, Willison RS, Kang M, Shen Y, Priest HD, Begemann MB, Cook KA, Bannon GA *et al.* 2021. Transgenic insertion of the cyanobacterial membrane protein *ictB* increases grain yield in *Zea mays* through increased photosynthesis and carbohydrate production. *PLoS ONE* **16**: e0246359.

Leegood RC. 1985. The intercellular compartmentation of metabolites in leaves of *Zea mays* L. *Planta* **164**: 163–171.

Leegood RC. 2002. C_4 photosynthesis: principles of CO_2 concentration and prospects for its introduction into C_3 plants. *Journal of Experimental Botany* **53**: 581–590.

Leegood RC. 2013. Strategies for engineering C_4 photosynthesis. *Journal of Plant Physiology* **170**: 378–388.

Littlejohn GR, Gouveia JD, Edner C, Smirnoff N, Love J. 2010. Perfluorodecalin enhances *in vivo* confocal microscopy resolution of *Arabidopsis thaliana* mesophyll. *New Phytologist* **186**: 1018–1025.

Liu Y, Dengler NG. 1994. Bundle sheath and mesophyll cell differentiation in the C_4 dicotyledon *Atriplex rosea*: quantitative ultrastructure. *Canadian Journal of Botany* **72**: 644–657.

Maai E, Nishimura K, Takisawa R, Nakazaki T. 2020. Light stress-induced chloroplast movement and midday depression of photosynthesis in sorghum leaves. *Plant Production Science* **23**: 172–181.

Maai E, Shimada S, Yamada M, Sugiyama T, Miyake H, Taniguchi M. 2011. The avoidance and aggregative movements of mesophyll chloroplasts in C_4 monocots in response to blue light and abscisic acid. *Journal of Experimental Botany* **62**: 3213–3221.

Mai KKK, Gao P, Kang BH. 2020. Electron microscopy views of dimorphic chloroplasts in C_4 plants. *Frontiers in Plant Science* **11**: 1020.

Muhaidat R, Sage TL, Frohlich MW, Dengler NG, Sage RF. 2011. Characterization of C_3–C_4 intermediate species in the genus *Heliotropium* L. (Boraginaceae): anatomy, ultrastructure and enzyme activity. *Plant, Cell & Environment* **34**: 1723–1736.

Ort DR, Merchant SS, Alric J, Barkan A, Blankenship RE, Bock R, Croce R, Hanson M, Hibberd JM, Long SP *et al.* 2015. Redesigning photosynthesis to sustainably meet global food and bioenergy demand. *Proceedings of the National Academy of Sciences, USA* **112**: 8529–8536.

Pignon CP, Lundgren MR, Osborne CP, Long SP. 2019. Bundle sheath chloroplast volume can house sufficient Rubisco to avoid limiting C_4 photosynthesis during chilling. *Journal of Experimental Botany* **70**: 357–365.

Ren T, Weraduwage SM, Sharkey TD. 2019. Prospects for enhancing leaf photosynthetic capacity by manipulating mesophyll cell morphology. *Journal of Experimental Botany* **70**: 1153–1165.

Seagull RW. 1983. Differences in the frequency and disposition of plasmodesmata resulting from root cell elongation. *Planta* **159**: 497–504.

Staehelin LA. 2003. Chloroplast structure: from chlorophyll granules to supramolecular architecture of thylakoid membranes. *Photosynthesis Research* **76**: 185–196.

Staehelin LA, Paolillo DJ. 2020. A brief history of how microscopic studies led to the elucidation of the 3D architecture and macromolecular organization of higher plant thylakoids. *Photosynthesis Research* **145**: 237–258.

Stata M, Sage TL, Rennie TD, Khoshravesh R, Sultmanis S, Khaikin Y, Ludwig M, Sage RF. 2014. Mesophyll cells of C_4 plants have fewer chloroplasts than those of closely related C_3 plants. *Plant, Cell & Environment* **37**: 2587–2600.

Still CJ, Berry JA, Collatz GJ, DeFries RS. 2003. Global distribution of C_3 and C_4 vegetation: carbon cycle implications. *Global Biogeochemical Cycles* **17**: 2001GB001807.

Stitt M, Heldt HW. 1985. Generation and maintenance of concentration gradients between the mesophyll and bundle sheath in maize leaves. *Biochimica et Biophysica Acta-Bioenergetics* **808**: 400–414.

Stitt M, Zhu XG. 2014. The large pools of metabolites involved in intercellular metabolite shuttles in C_4 photosynthesis provide enormous flexibility and robustness in a fluctuating light environment. *Plant, Cell & Environment* **37**: 1985–1988.

Théroux-Rancourt G, Earles JM, Gilbert ME, Zwieniecki MA, Boyce CK, McElrone AJ, Brodersen CR. 2017. The bias of a two-dimensional view: comparing two-dimensional and three-dimensional mesophyll surface area estimates using noninvasive imaging. *New Phytologist* **215**: 1609–1622.

Turrell FM. 1936. The area of the internal exposed surface of dicotyledon leaves. *American Journal of Botany* **23**: 255–264.

Walker BJ, VanLoocke A, Bernacchi CJ, Ort DR. 2016. The costs of photorespiration to food production now and in the future. *Annual Reviews Plant Biology* **67**: 107–129.

Wang Y, Long SP, Zhu XG. 2014. Elements required for an efficient NADP-malic enzyme type C_4 photosynthesis. *Plant Physiology* **164**: 2231–2246.

Weise SE, Carr DJ, Bourke AM, Hanson DT, Swarthout D, Sharkey TD. 2015. The *arc* mutants of *Arabidopsis* with fewer large chloroplasts have a lower mesophyll conductance. *Photosynthesis Research* **124**: 117–126.

Wingler A, Walker RP, Chen ZH, Leegood RC. 1999. Phosphoenol pyruvate carboxykinase is involved in the decarboxylation of aspartate in the bundle sheath of maize. *Plant Physiology* **120**: 539–546.

Xu D, Cui J, Bansal R, Hao X, Liu J, Chen W, Peterson BS. 2009. The ellipsoidal area ratio: an alternative anisotropy index for diffusion tensor imaging. *Magnetic Resonance Imaging* **27**: 311–323.

Yan D, Yadav SR, Paterlini A, Nicolas WJ, Petit JD, Brocard L, Belevich I, Grison MS, Vaten A, Karami L *et al.* 2019. Sphingolipid biosynthesis modulates plasmodesmal ultrastructure and phloem unloading. *Nature Plants* **5**: 604–615.

Zhang X, Liang Y, Song X, Wang Z, Zhang B, Lei J, Li Y, Yan M. 2021. Changes in gene expression levels and chloroplast anatomy induced by *Leifsonia xyli* subsp. *xyli* in sugarcane. *Journal of Plant Interactions* **16**: 564–574.

Zhu XG, Hasanuzzaman M, Jajoo A, Lawson T, Lin R, Liu CM, Liu LN, Liu Z, Lu C, Moustakas M *et al.* 2022. Improving photosynthesis through multidisciplinary efforts: the next frontier of photosynthesis research. *Frontiers in Plant Science* **13**: 967203.

Supporting Information

Additional Supporting Information may be found online in the Supporting Information section at the end of the article.

Fig. S1 Workflow for tracing plasmodesmata pit fields.

Fig. S2 Images of bundle sheath and mesophyll cells plasmodesmata in sugarcane and maize leaf samples.

Fig. S3 Attempted tracing of individual plasmodesmata through the pit field in sugarcane.

Fig. S4 Chloroplast volume distribution in bundle sheath and mesophyll cells.

Fig. S5 Comparison of bundle sheath cell diameter as determined by laser scanning microscopy and serial block face scanning electron microscopy collected from the same leaf area in sugarcane.

Fig. S6 3D visualization of two bundle sheath cells interconnecting.

Fig. S7 Sugarcane leaf cross section viewed perpendicular to the midvein.

Table S1 Characteristics of mesophyll chloroplasts in maize and sugarcane measured by laser scanning microscopy.

Table S2 Mean pit field count for the observable surface area of the bundle sheath cells for both maize and sugarcane.

Table S3 Laser scanning microscopy estimates of cell length from Danila *et al.* (2016) and Fig. S7 with estimated chloroplast number per cell using Table 2 data.

Please note: Wiley is not responsible for the content or functionality of any Supporting Information supplied by the authors. Any queries (other than missing material) should be directed to the *New Phytologist* Central Office.